High Power Arcjet

M. Auweter-Kurtz, B. Glocker, T. M. Gölz,
H. Habiger, H. L. Kurtz, H. O. Schrade, T. Wegmann

Institut für Raumfahrtsysteme
University of Stuttgart
IRS 90–P7

Second Progress Report
NASA Grant No. NAGW–1736
for NASA Lewis Research Center, Cleveland, OH

August 1990

Contents

Abstract

This second progress report covers the activities on the development of the high power arcjet HIPARC, the thrust balance, and plasma diagnostic probes from November 1989 to July 1990.

Modifications of the HIPARC design and a synopsis of the materials used are given. Further experimental results with the TT30 thruster in the 50 kW range are presented.

Some first calibration measurements of the thrust balance are also included. Progress concerning the development of plasma diagnostic devices is documented.

1 High Power Arcjet Thruster

1.1 Modifications

The final High Power Arcjet (HIPARC) design differs in several points from the design presented in the first progress report:

1. Due to your proposal (Fax dated March, 14th 1990) the nozzle contour was changed from bell to conical shape, with a 20 degree half-angle. This results in a new A_e/A_t ratio of 114, which is greater than it had been before (100).
2. Propellant was changed from ammonia to hydrogen.
3. The maximum mass flow rate has been reduced from 1 g/s to 0.5 g/s.
4. Due to experimental results with the TT30 thruster the throat diameter was reduced to 6 mm, which is still supposed to be rather big.
5. In order to perform current distribution measurements, all segments are now supplied with power individually, each having in-line a shunt resistor for current measurements.
6. A pressure tap has been included to determine the chamber pressure.
7. For easy variation of the propellant injection the injector consists of four molybdenum inserts, which are easy to replace in order to check different injection angles and bore hole diameters.

Fig. 1 shows a cross sectional drawing of the HIPARC thruster. In Picture 2 the thruster can be seen prior to integration into the vacuum chamber.

1.2 Materials Used

All electrical conducting parts as the cathode tube and the nozzle segments are made of copper. The cathode itself is made of 2 %-thoriated tungsten. The arc chamber consists of steatite, containing four molybdenum inserts serving as propellant injectors.

The cathode positioning device is based on an aluminum part which is beared on a polyvinyl chloride (PVC) traverse. The cathode tube housing, the segment base plate and the gasket elements between the nozzle segments are also made of PVC. PTFE (polytetraflouroethylene) is the material of which the socket shells are made.

In Fig. 3 the materials can be distinguished by different colours.

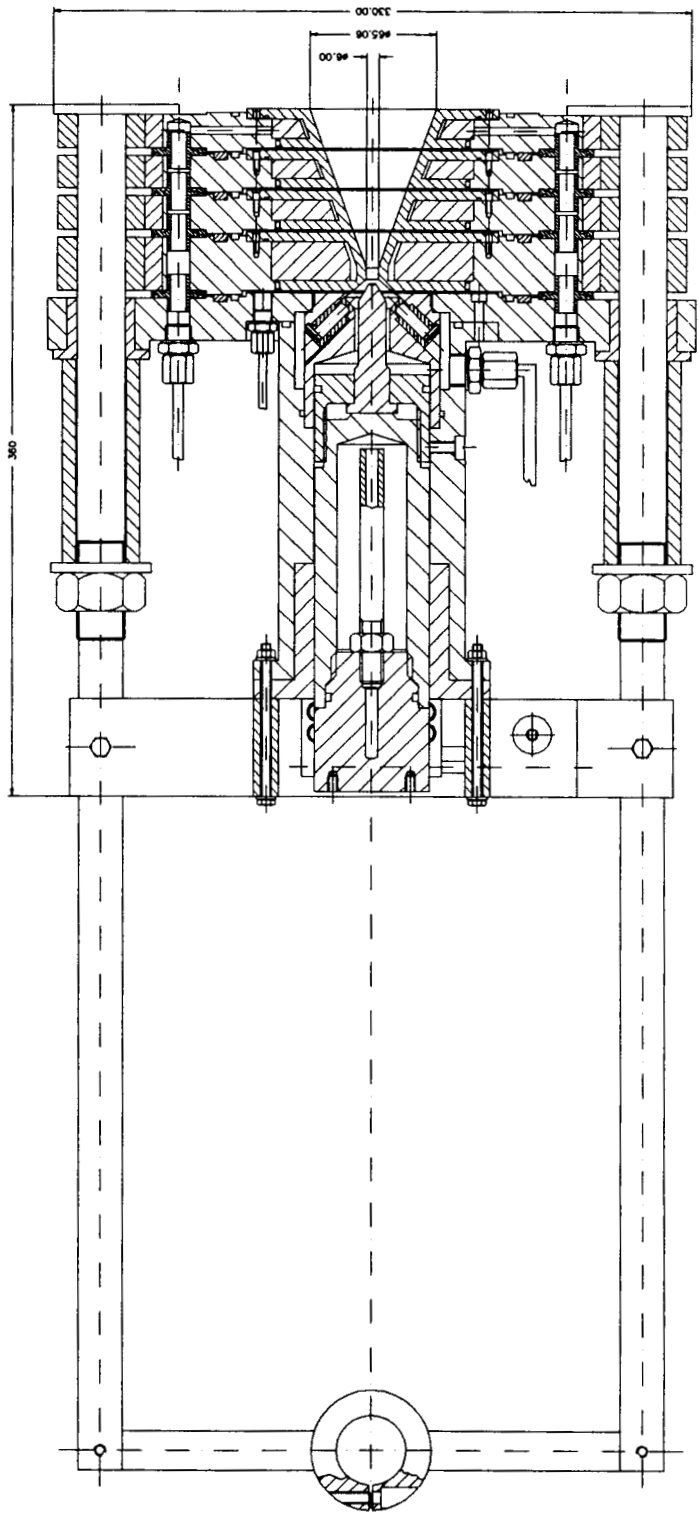

Figure 1: HIPARC Cross Sectional Drawing

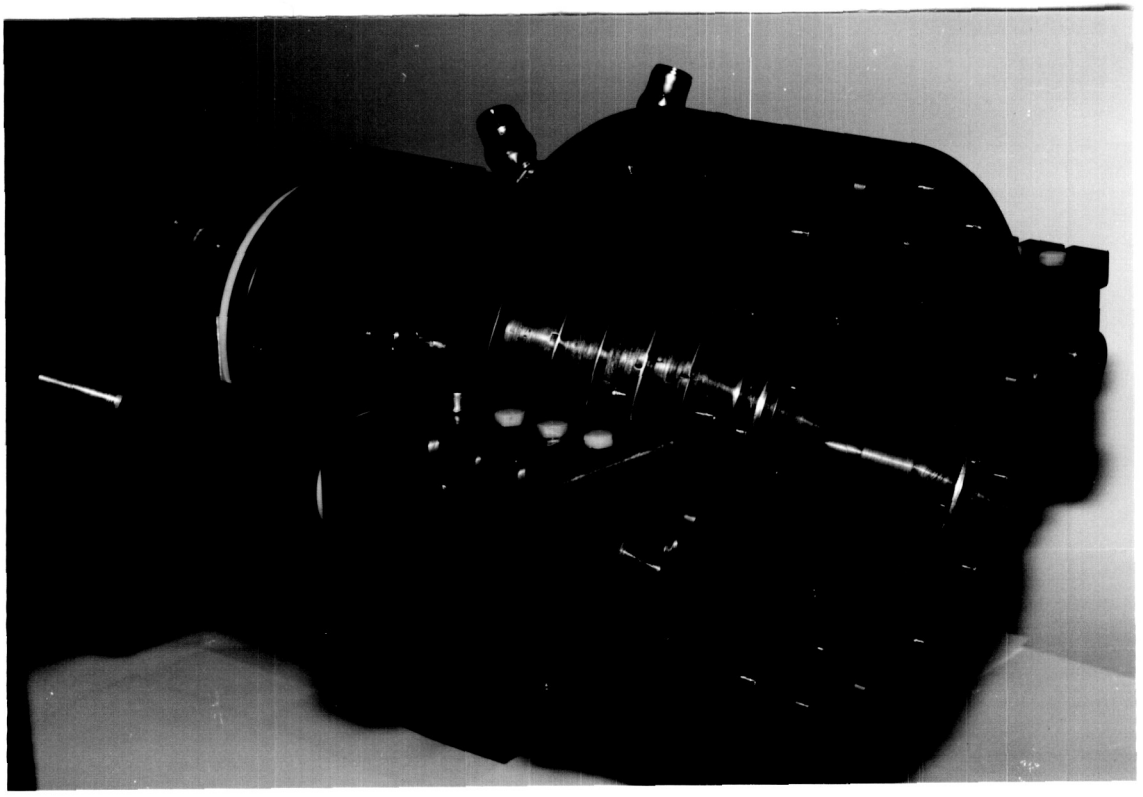

Picture 2: HIPARC Thruster

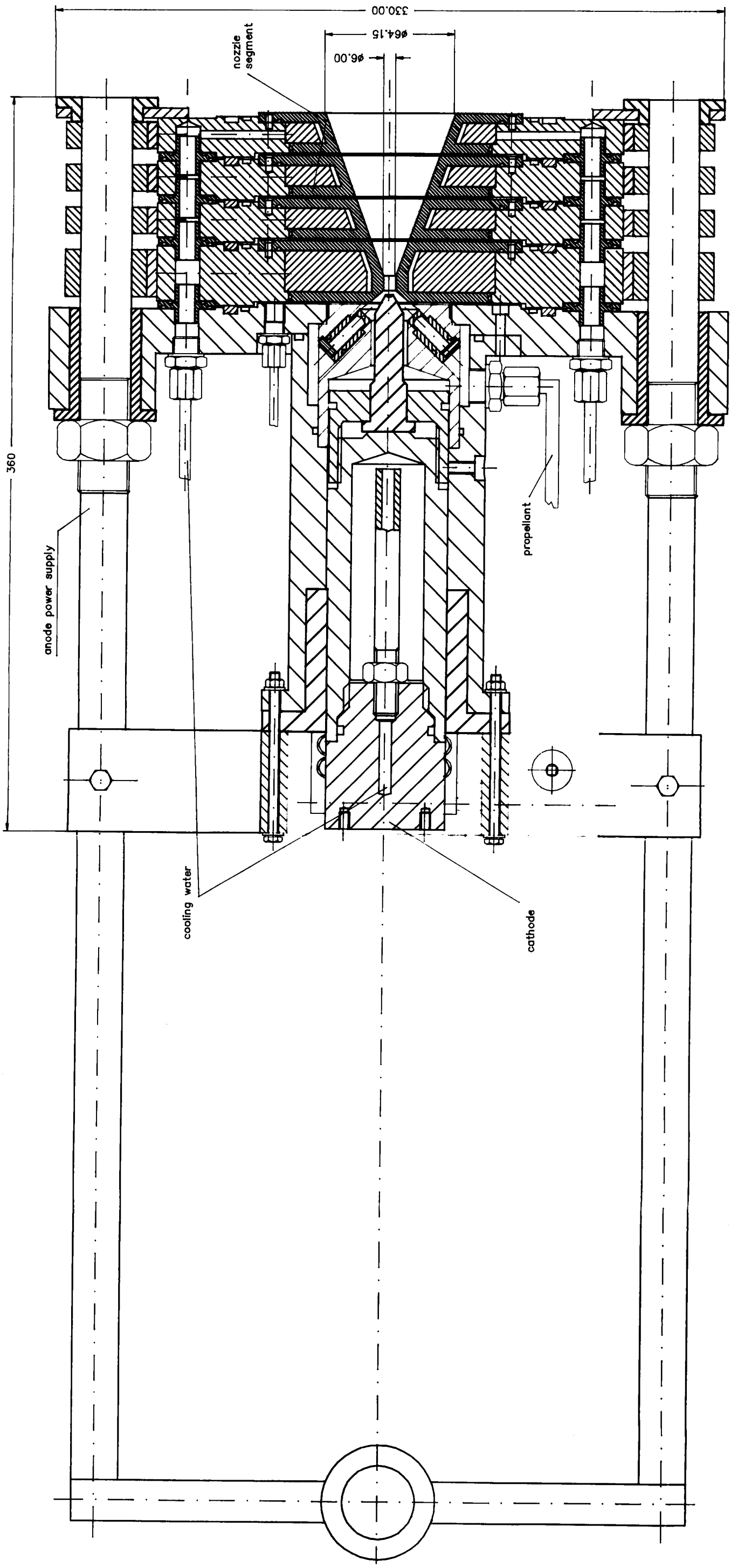

Figure 3: Materials: copper (orange), thoriated tungsten (red), molybdenum (purple), aluminum (brown), steatite and other ceramics (green), polyvinyl chloride (blue), PTFE (light blue), other materials (black)

2 TT30 – Further Experimental Results

As the experiments described in the first progress report were limited to a 400 A current by the facility, the facility has been rebuilt, so that the current limit is now at 1000 A. With this rebuilt facility tests were performed with hydrogen as propellant and mass flow rates of 0.1 g/s, 0.2 g/s, and 0.3 g/s, using the 5 mm throat diameter and the 2 mm cathode gap. In the case of the two lower mass flow rates the thruster was not operated to its limits, whereas with 0.3 g/s 430 A was shown to be the maximum current for the cathode of 4 mm diameter. With a mass flow rate of 0.1 g/s, a specific impulse of more than 750 s can be reached, whereas with 0.3 g/s it is limited due to the small cathode to about 600 s. The efficiencies are rather low, between 10 % and 16 %, increasing with higher mass flow rates and decreasing with higher power. With a propellant flow of 0.3 g/s more than 50 kW could be reached without any damage of the nozzle segments (Fig. 6). The arc chamber pressure was never higher than 900 mbar (Fig. 6), and the heat flux was moderate (Fig. 8). The major part of the heat flux was deposited into the first two segments downstream of the nozzle throat which served as anodes (Fig. 8), whereas the heat load of the nozzle throat was always less than 0.37 kW/cm^2.

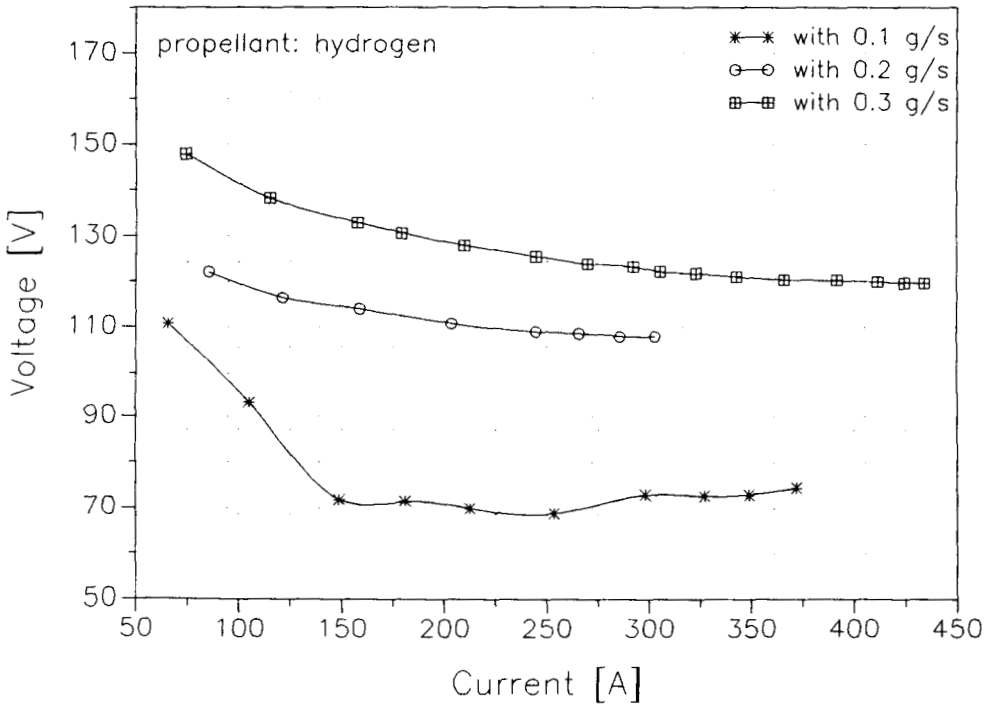

Figure 4: Current - Voltage Characteristic

These results indicate that specific impulse and efficiency can be improved at higher power levels using a thicker cathode.

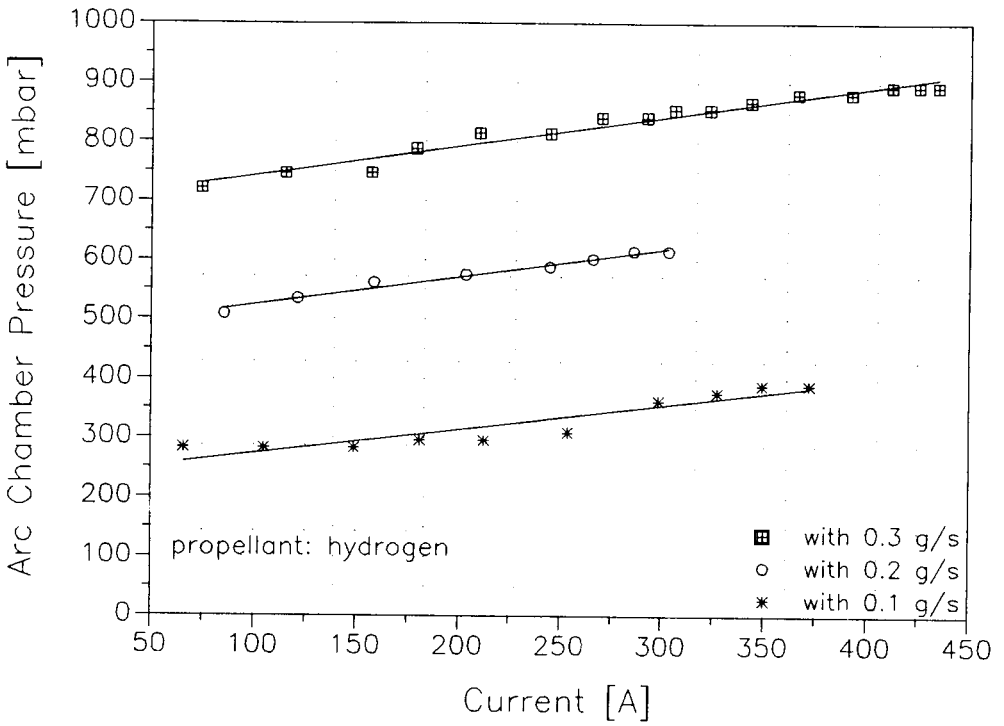

Figure 5: Current - Arc Chamber Pressure Characteristic

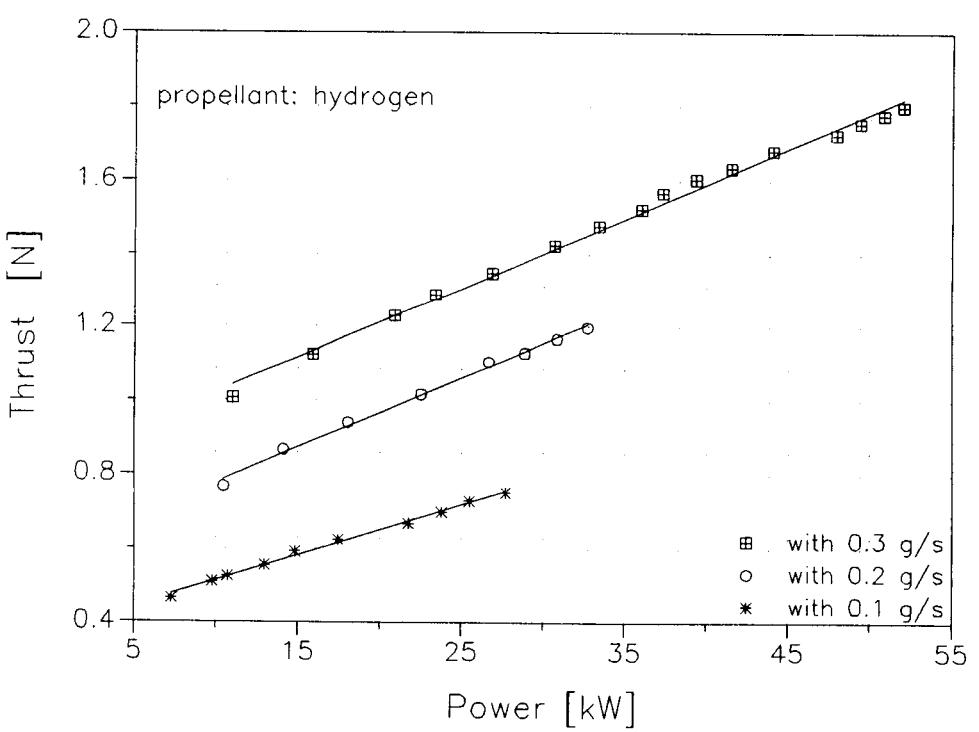

Figure 6: Power -Thrust Characteristic

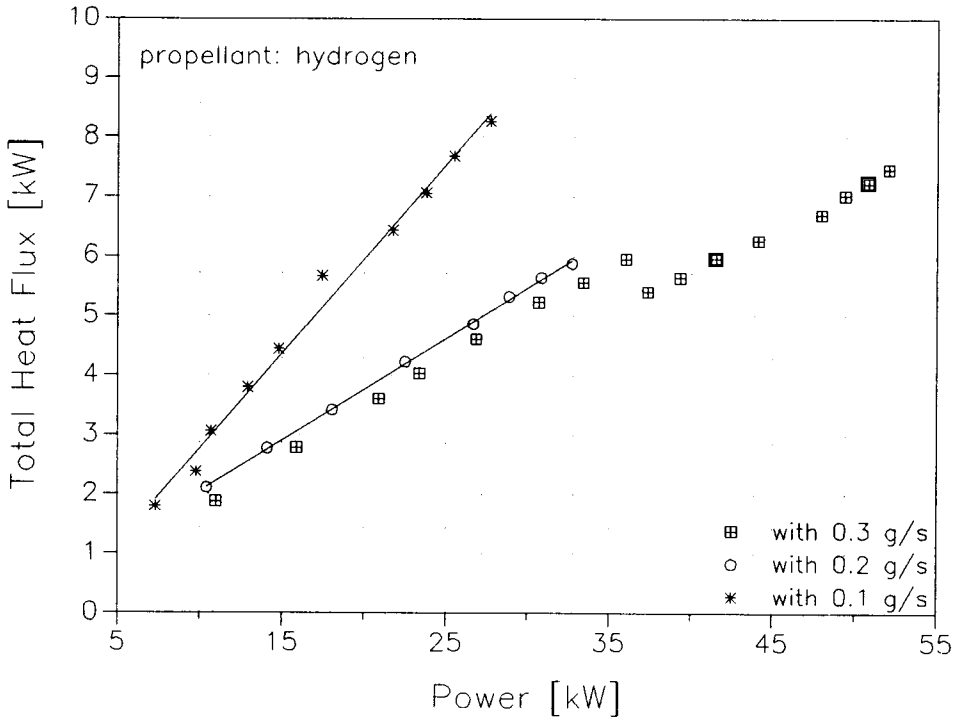

Figure 7: Power - Heat Flux Characteristic

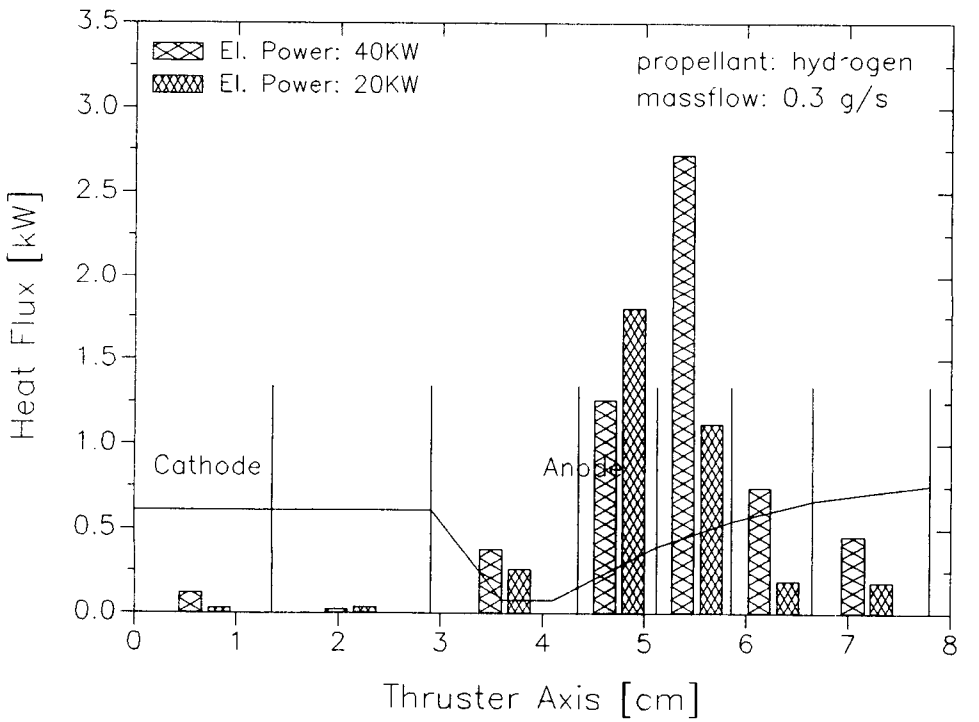

Figure 8: Heat Flux Distribution

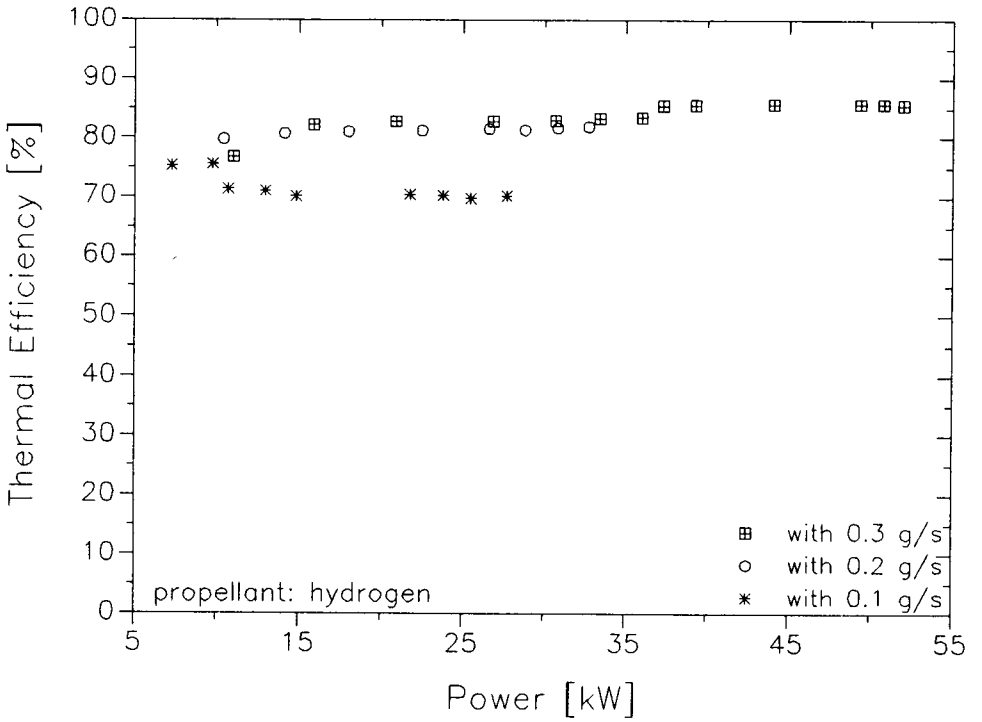

Figure 9: Thermal Efficiency vs. Input Power

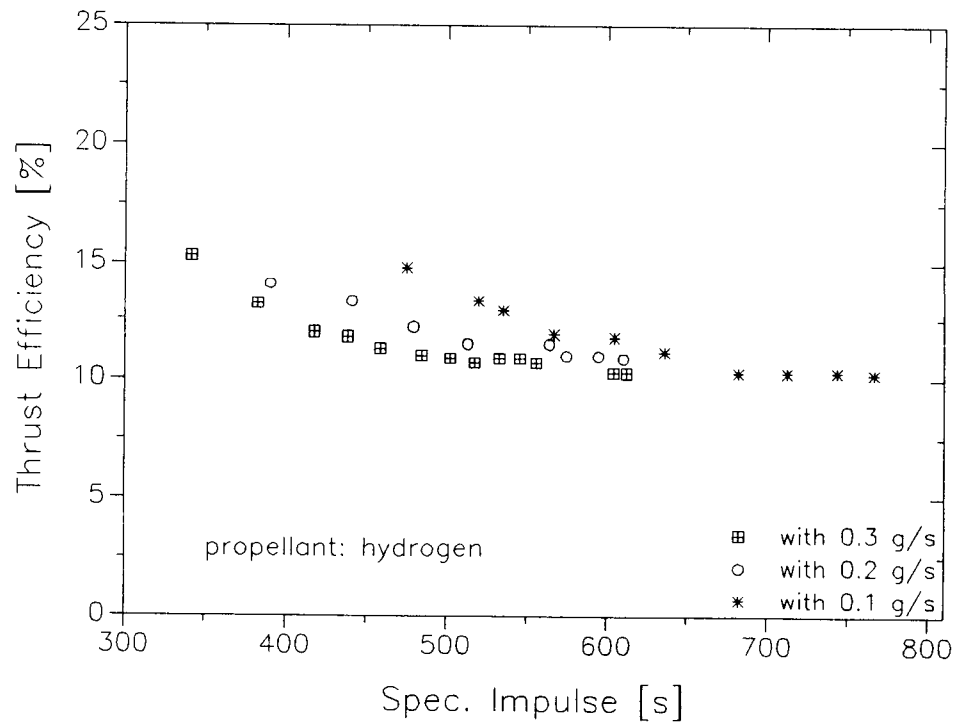

Figure 10: Efficiency vs. Specific Impulse

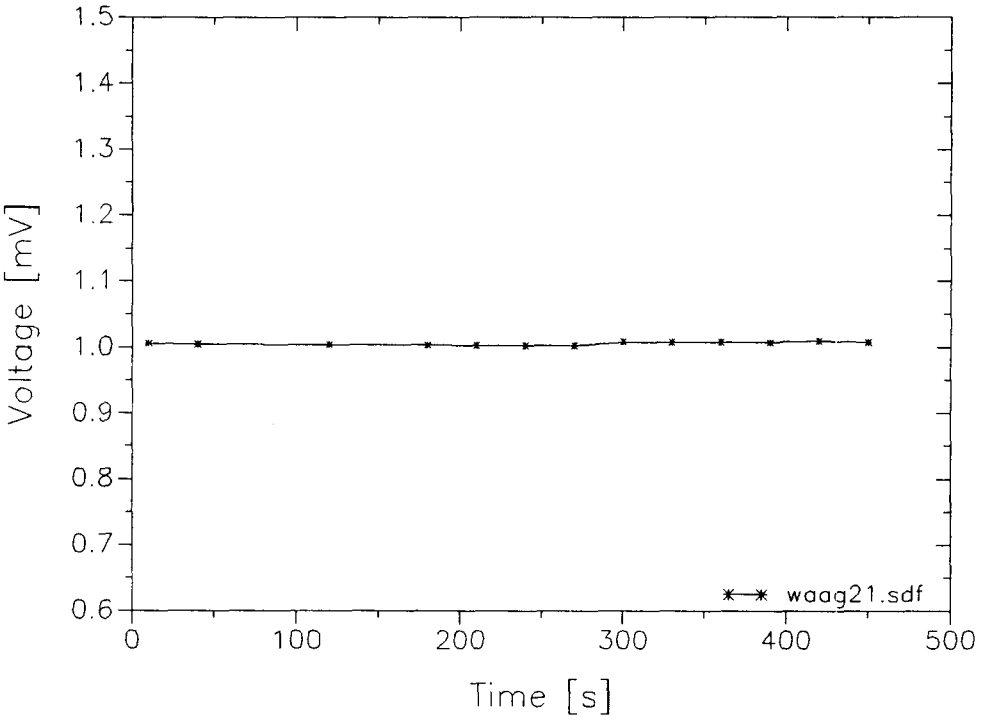

Figure 11: Voltage vs. Time During Heat-Up and Cool-Down

3 Test Facilities

3.1 Thrust Balance

The thrust balance has been mounted and integrated in the vacuum chamber. First calibration measurements have been carried out without the thruster being mounted. The influence of temperature was simulated by heating critical parts by a hot air blower. During the heat-up and cool-down process balance data was recorded with constant weight on the balance. Fig. 11 shows the voltage vs. time characteristics for this case.

Several datasets have been recorded to determine performance characteristics, each set beginning with zero weight, increasing weight successively up to $\approx$ 600 g, and subsequently decreasing weight successively down to zero. Different initial stress values resulting in different zero-weight voltages have been established. As Fig. 12 shows, linear characteristics can be achieved by reasonable initial stress only.

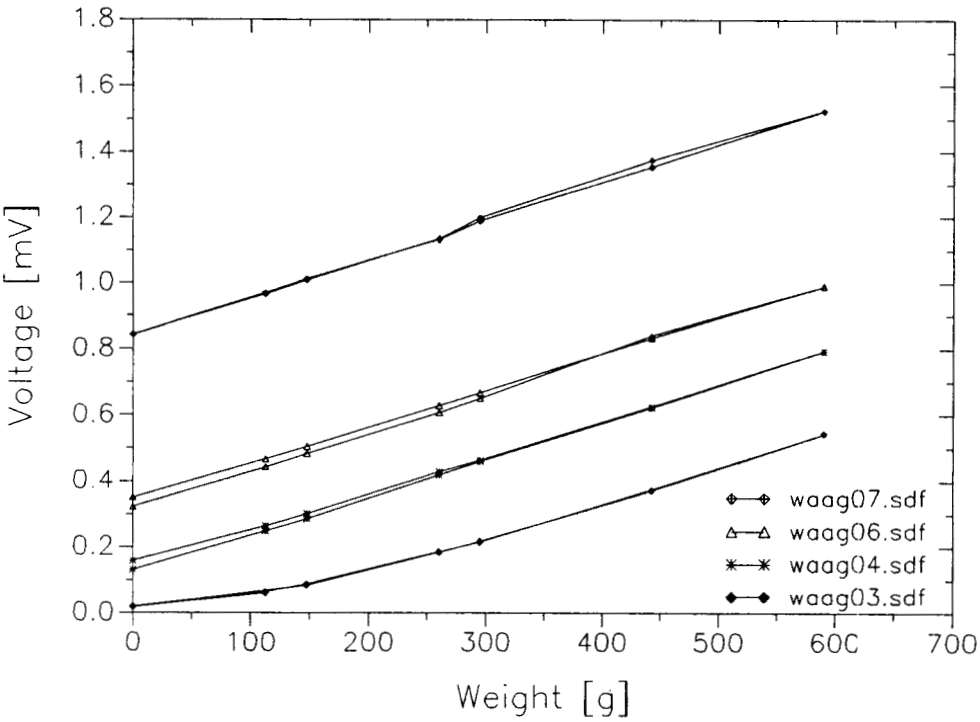

Figure 12: Voltage vs. weight characteristic at different initial stress values, showing one load/release-cycle each.

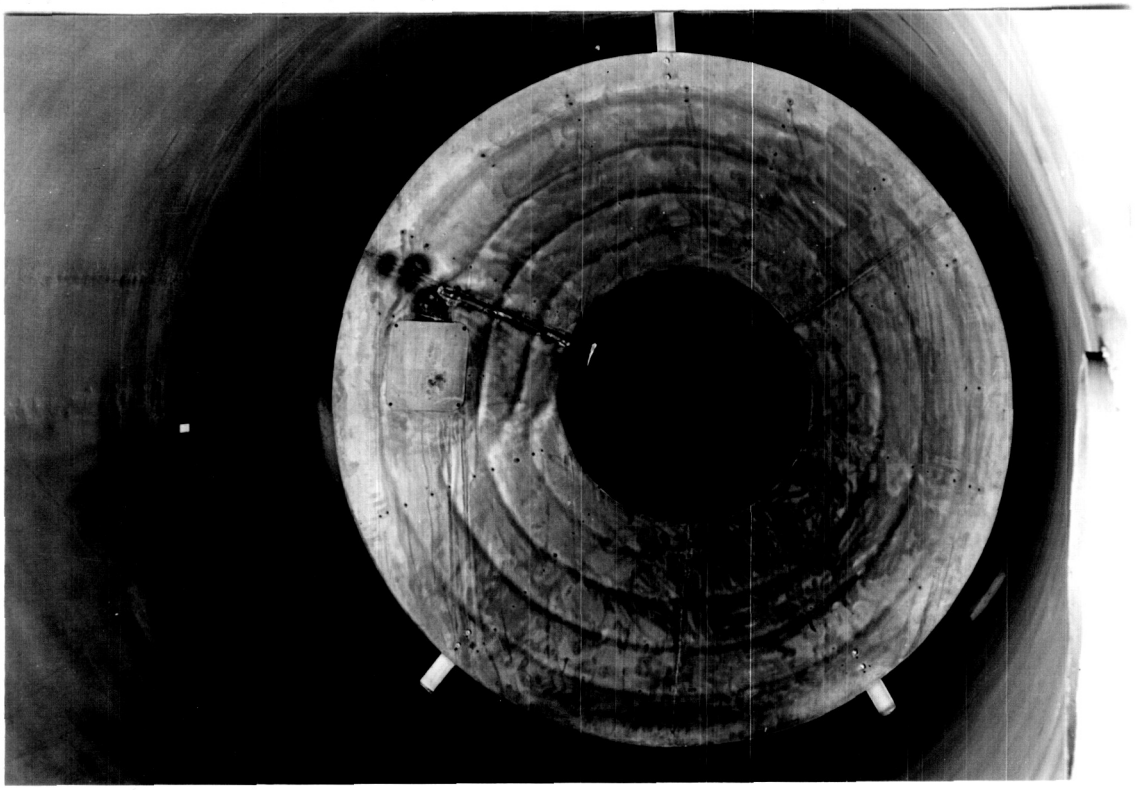

Picture 13: Gas Cooler

3.2 Vacuum Tank Preparation

The thrust balance has been integrated into the vacuum tank. New feed-through power supply leads have been installed, because the old ones didn't fit the new thrust balance.

In order to avoid thermal overload of the vacuum system, a gas cooler has been built in just in front of the outlet (Fig. 13).

3.3 Gas Supply System

Since the gas supply system was limited to a maximum mass flow rate of 0.3 g/s hydrogen, a new mass flow controller with a range of 0–0.5 g/s hydrogen has been integrated.

3.4 Data Acquisition System

In order to perform current distribution measurements, three additional isolation amplifiers have been installed, each of them leading to our DEC PDP-11/73 data

acquisition computer via newly installed ADC channels on our Intercole Spectra data acquisition system.

4 Fabry-Perot-Interferometry

With the FPI, it is planned to measure Doppler-shifts of spectral emission lines of an accelerated plasma and therefore the velocities of the emitting particles. The temperatures of the heavy particles can also be measured from the Doppler broadening of the emission lines. The technical concept of the FPI was already described in detail in the former progress report [1].

The experimental setup of the Fabry-Perot-Interferometry has now been build up. It is shown in pictures 15 and 16 and can be compared to figure 14.

Picture 15 shows the optical rack on the left hand side and the data acquisition rack on the right. The data acquisition rack includes the computer and the the transient recorder on the two lower levels. The optical rack which is shown in more detail in picture 16, is divided into four levels. On the upper level, the reference light sources and collimating optics are mounted. The reference light passes through a hole down to the second levels, where the light collecting optics are mounted. The silver colored assembly on the left includes the collecting optics and the beam splitter. By several plane mirrors, the light is passed through the FPI which is on the right hand side. After the FPI an additional mirror reflects the light to the third level with the focussing lens, the narrow band filter and the photomultiplier. The fourth level includes the power supply for the photomultiplier and the ramp generator for the FPI. The whole rack is mounted on a marble block in order to suppress vibrations which will disturb the FPI calibration. At the moment only a slight effort is done to suppress external vibrations.

At the moment the calibration of the optics without the mirror plates of the FPI is being performed. In a second step the mirror plates will be mounted and the effect of external vibrations on the setup will be examined. Depending on the results the most effective vibration isolation has to be installed in order to perform measurements. It is planned to start reliable operation of the FPI in spring 1991.

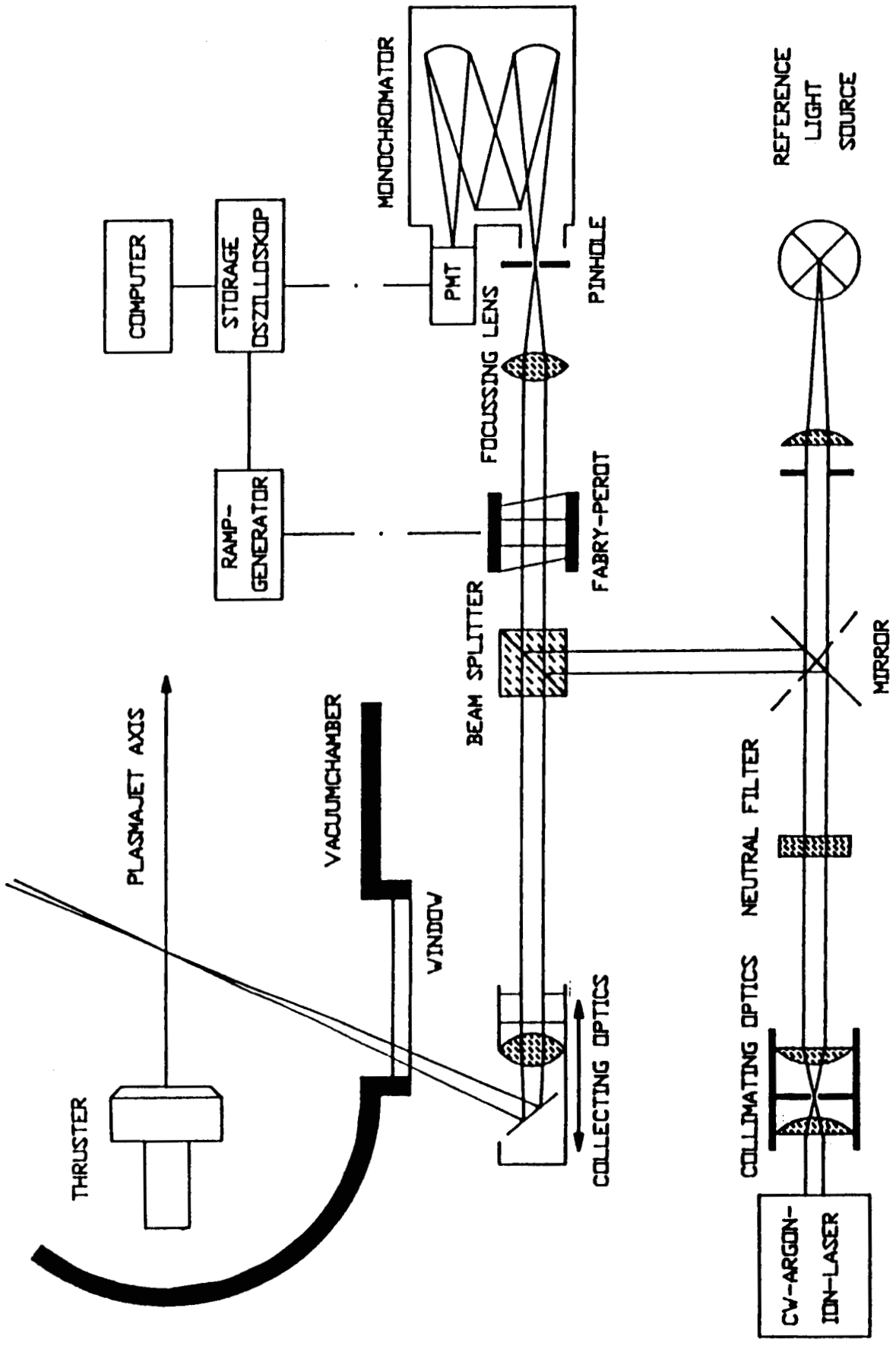

Figure 14: Schematic Drawing of the Fabry-Perot Interferometry

Picture 15: FPI: Apparatus

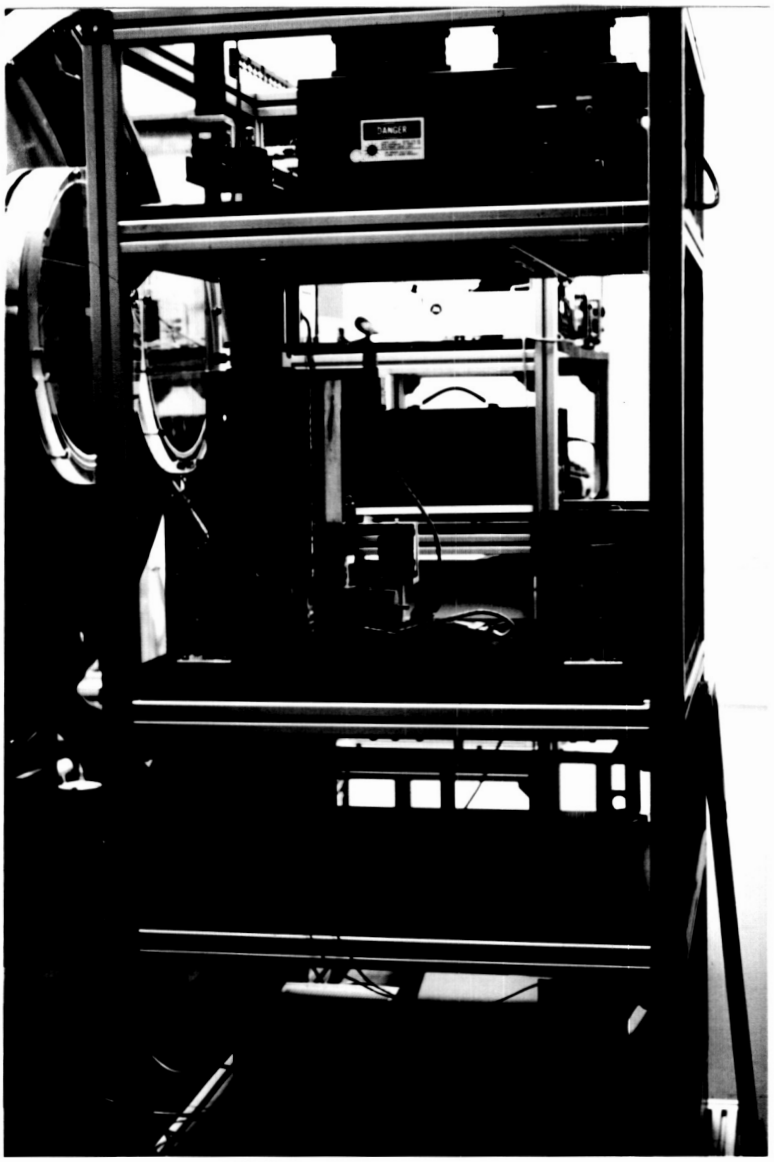

Picture 16: FPI: Optical Rack

5 Plasmadiagnostics with Electrostatic Probes at the IRS

With means of electrostatic probes, we want to measure the distributions of the electron temperatures and electron densities in our plasma-jets, as well as the velocities of the plasma particles by time-of-flight measurements. The directions of the plasma-streamlines can also be detected with electrostatic probes by measurements of the ion-current at different angles of attack.

5.1 Measurements of Electron Temperature and Density with Triple-Probes

Electrostatic triple-probes are used to determine the values of the electron temperature and the electron density instantaneously, within a short time on the order of the probe response time. Several triple probes of different dimensions are being built up. The technical concept of the probes was described in the former progress report [1].

First measurements of the electron temperature were performed with the DT2 and the ZT1 MPD-thrusters of the IRS. While the data acquisition works convenient, the xy-table which moves the triple probe through the plasma jet causes some problems. The maximum speed of the xy-table in radial position is about 4 cm/s. By typical jet diameters of 20 to 40 cm depending on the ambient pressure, the movement through the jet plume takes 5 to 10 seconds. Figure 18 shows a radial profile of the electron temperature of the DT2 plasma plume. The triple probe was moved from the left to the right. Despite the reproducable shape of T_e at reasonable values in the center of the plasma plume, one can clearly see a small maximum of T_e at a position of about –85 mm which does not occur symmetrically. Also there is an remarkable rise of T_e in the outer regions of the jet after the probe was moved through. Such a behavior occured also when we moved the probe from the right to the left as one can see in Figure 19. The appearence of such a maximum also has been detected before the probe reaches the jet axis in the ZT1 thruster (see Figure 20). Besides the fact that the absolute values of T_e are affected by different angles of attack in the outer regions of the plasma jet, it is supposed that the behavior of the probes is caused by heating effects. To avoid those heating effects, it is planned to build up a faster xy-table. The radial movement of the new table should be driven by a pendulum to reach speed of about 20 to 30 cm/s. The new table will be operational until November.

Picture 17 shows the triple probe during operation in argon.

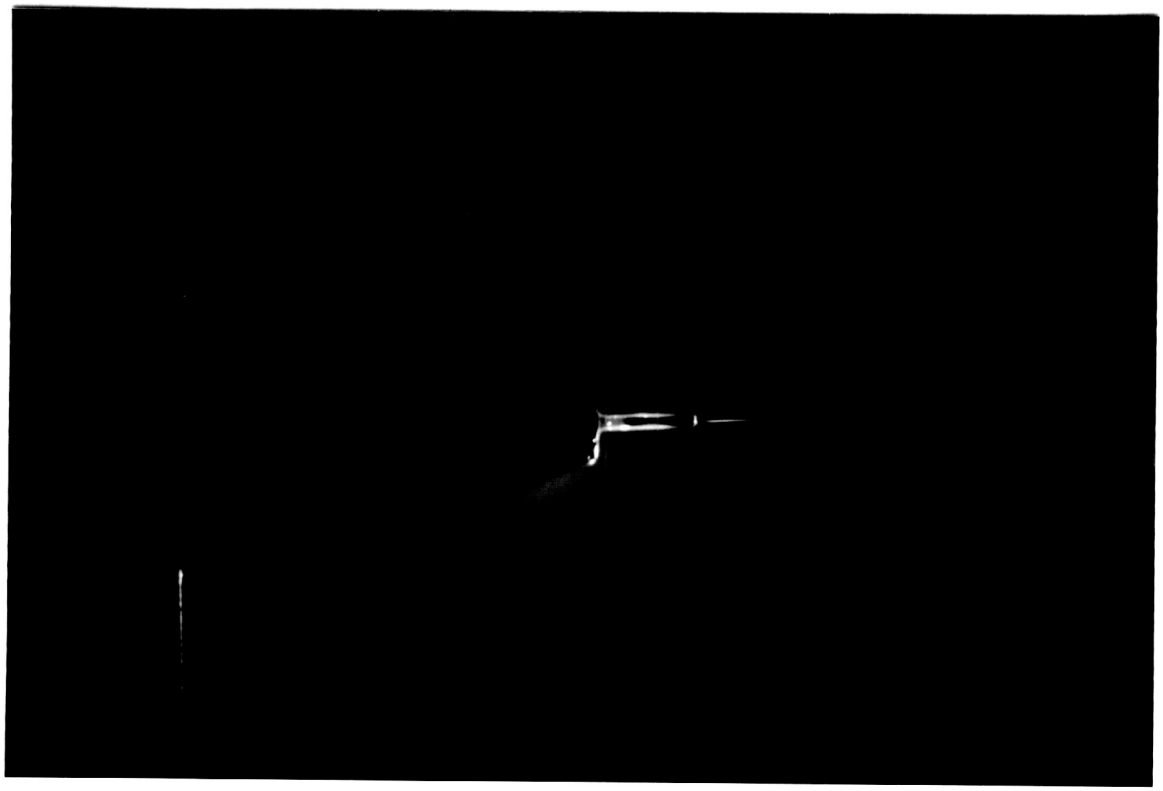

Picture 17: Triple-Probe Measurement

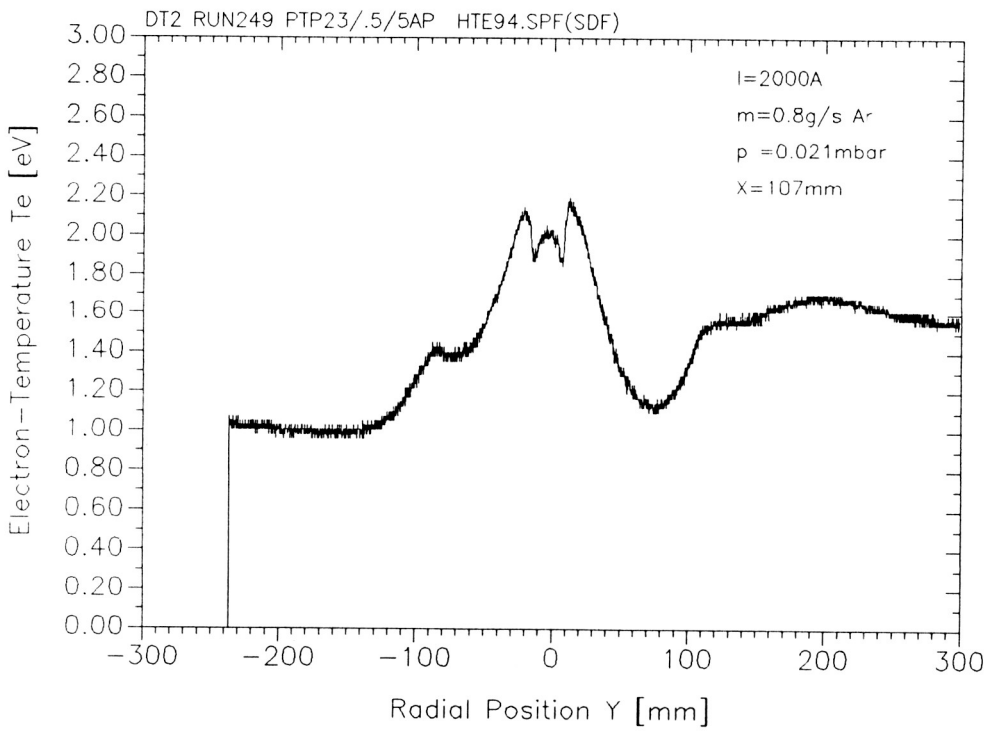

Figure 18: Radial Distribution of the Electron Temperature (I)

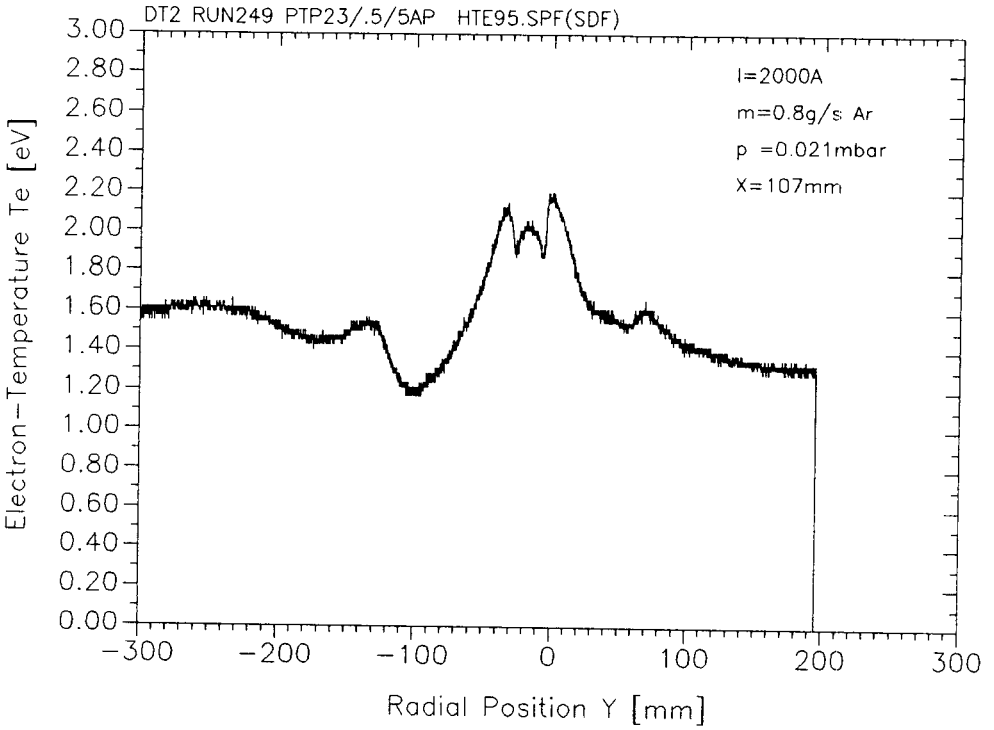

Figure 19: Radial Distribution of the Electron Temperature (II)

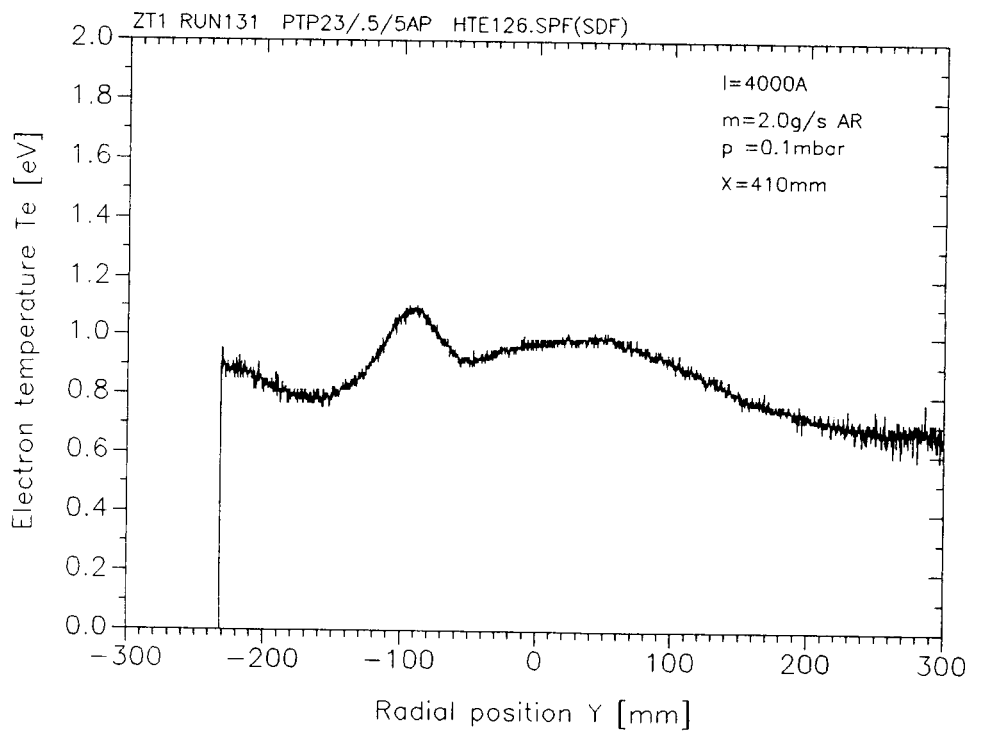

Figure 20: Radial Distribution of the Electron Temperature (III)

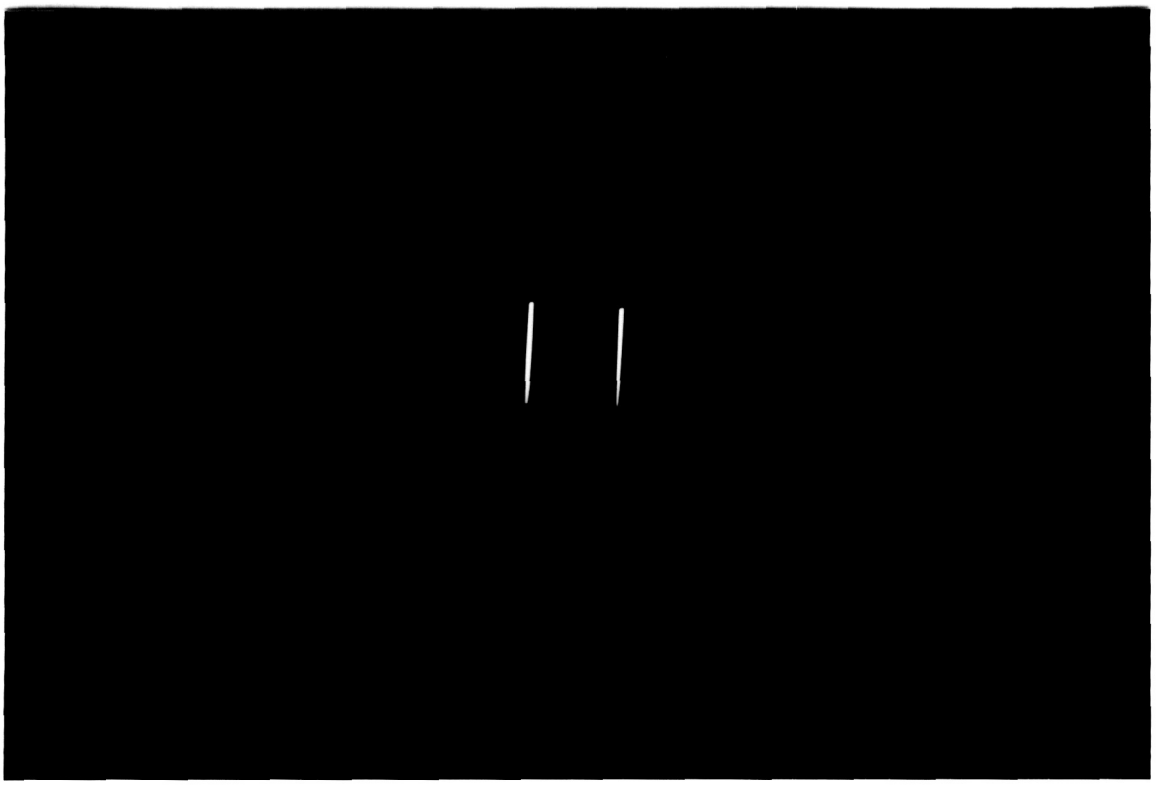

Picture 21: Time-of-Flight Probe

5.2 Measurement of Plasma Velocities with Time-of-Flight Probes

The technical concept for time-of-flight measurements of natural plasma fluctuations was also described in the last progress report.

A first student thesis on the time-of-flight measurement of natural fluctuations has been performed with the DT2 and the ZT1 MPD-thrusters. The major result of the thesis is, that the density of charged particles at low massflows and high currents seems to be very large at the center axis of the plasma jet. So far the natural fluctuations are not clearly marked and difficult to detect. For the investigated thruster parameters, the method seems to allow only a rough estimation of the plasma speed. The next step of the time-of-flight measurement will be to generate fluctuations and to detect plasma streamlines for probe axis alignment. Picture 21 shows the time-of-flight probe during operation.

6 Optical Diagnostics

During the designing and construction phase of the high power arcjet and its test stand, the qualification of the optical plasma diagnostics have been continued. For that purpose especially emission spectroscopic measurements were carried out both at the arcjets of lower power and at MPD-thrusters. First of all general spectra for different propellants and various operating conditions were taken. These are important for the line identification and to determine the different plasma parameters from the line broadening and the Doppler shift of selected emission lines subsequently. An Abel inversion technique is being installed for the determination of the plasma parameters at different radial positions from the measured radial emission profiles.

The measured general spectra at the nozzle type magnetoplasmadynamic (MPD) thruster of the DT-series yielded to new results concerning the onset-phenomena, where various instabilities of the arc and the plasma flow appear which limit the high power levels of these devices. Figure 22 shows the voltage versus current curve of the MPD-thrusters running with argon as propellant. These curves rise steeply at high power levels ($\approx$ 4200 A), which results in a decrease of the thrust efficiency. At a current level somewhat above this break in the voltage curve, oscillations of the plasma can be detected in low and high frequency ranges, Fig. 23, which can be measured with an electrical probe. Figures 24–27 show spectroscopic measurements, done at the MPD-thruster DT2-IRS running with 0.8 g/s argon at different current levels, between 2700 A and 3500 A. These measurements show that already at current levels of about 3000 A, spectral lines of the second ionized argon appear and so at least in the core of the plasma plume the second ionization of the argon atoms starts.

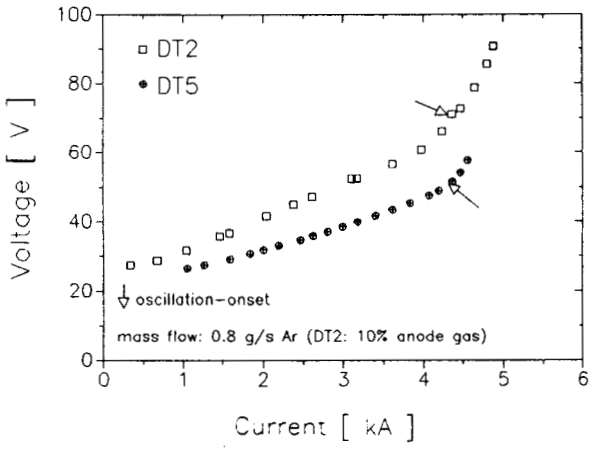

Figure 22: Voltage vs. current of the MPD-thrusters DT2 and DT5, running with 0.8 g/s argon, arrows indicating the onset of oszillations

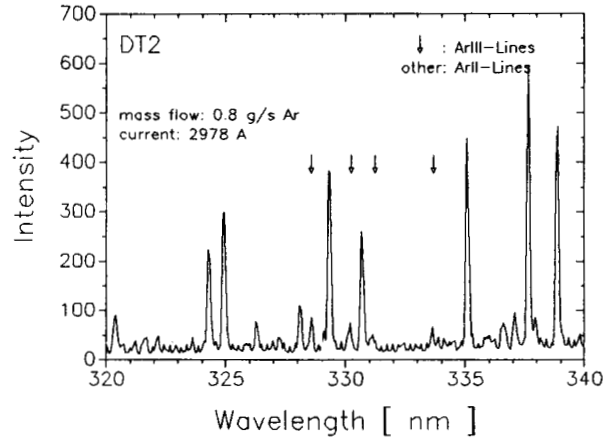

Figure 25: Intensity vs. Wavelength at 2978 A

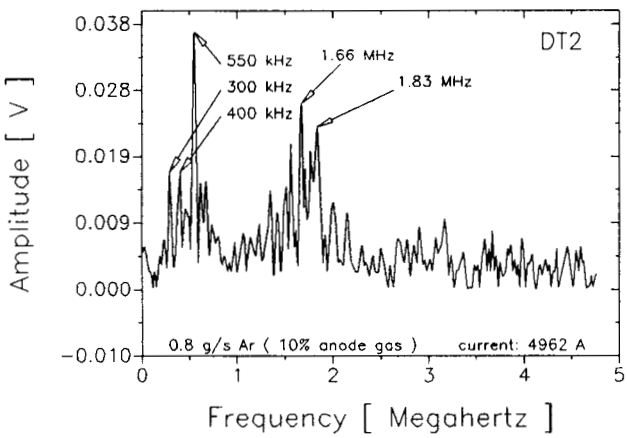

Figure 23: Frequency Spectrum of the Plasma Oscillations at the DT2-Thruster

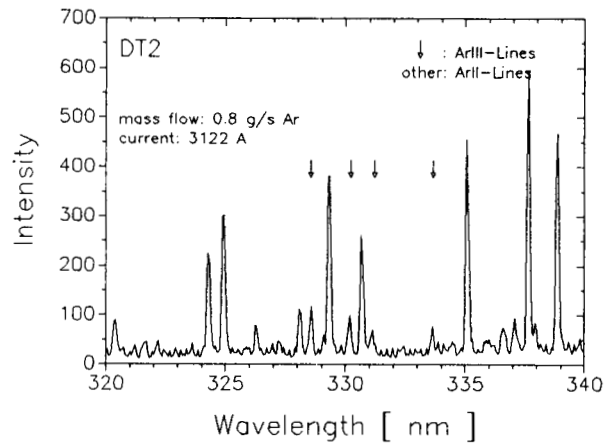

Figure 26: Intensity vs. Wavelength at 3122 A

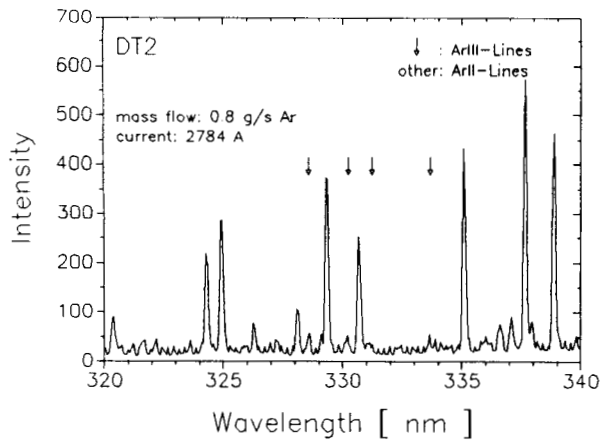

Figure 24: Intensity vs. Wavelength at 2784 A

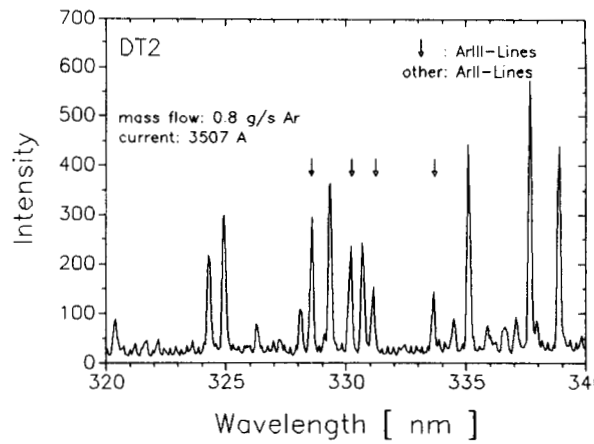

Figure 27: Intensity vs. Wavelength at 3507 A

References

[1] HIPARC, High Power Arcjet, M. Auweter-Kurtz et al., Institut für Raumfahrtsysteme, University of Stuttgart, IRS 89-P19, First progress report, NASA Grant No. NAGW–1736, October 1990